Plasma state transition originating from local production of massive negative ions

Wataru Oohara and Rikizo Hatakeyama
Department of Electronic Engineering, Tohoku University, Sendai 980-8579, Japan

Seiji Ishiguro
Theory and Computer Simulation Center, National Institute for Fusion Science, Toki 509-5292, Japan
(Received 16 August 2003; published 31 December 2003)

A dynamic evolution of plasma structures and its associated state transition due to local production of massive negative ions are investigated by the particle-in-cell simulation which is based on an experimental configuration of an open plasma system (Q machine). Two different states, a stationary state and a dynamic state, are achieved depending on the production rate of massive negative ions. The plasma is stationary for a low production rate, while solitary pulses and fluctuations are spontaneously excited and the plasma state is unstable for a high production rate. Phenomena of a two-stream instability and a double layer formation induced by the local production are closely concerned with the excitation of the solitary pulse. The solitary pulses play a role in the rapid ejection of massive negative ions from the system. A staying time distribution of charged particles is analogically introduced for the special convenience of explanation, which corresponds with a so-called population pyramid. The staying time distribution can clearly express the feature of the state since all the phenomena occurring in the system directly reflect the distribution.

DOI: 10.1103/PhysRevE.68.066407 PACS number(s): 52.35.Mw, 52.27.Cm, 52.35.Qz, 52.65.Rr

I. INTRODUCTION

Recently it has widely been recognized that plasmas containing dust or fine particles are a subject of intensive study in various fields of physics and engineering such as space astrophysics [1–3], plasma physics [4–6], plasma-aided manufacturing [7–9], and fusion technology [10–13]. In that connection, the crucial concern is that fine particles play important roles in wave propagation, instability, particle transport, confinement, contamination, plasma condensation, and structural formation of nanoscopic and microscopic sizes. As these fine particles are often negatively charged in low-temperature plasmas, massive negative ion plasmas are confirmed to exist in many natural and technological setting. Therefore, it is basically important to investigate effects of negative ion production on microscopic and macroscopic plasma structures. Negative ion plasmas have been produced in laboratories by various methods in order to investigate wave and instability phenomena [14] related to fine-particle space plasmas. In most cases, the method based on an attachment of low-energy electrons to species such as SF_6 (mass number $\simeq 146$) and $CFCl_3$ (mass number$\simeq 137$) has been adopted exclusively to carry out laboratory wave experiments, where the production region of negative ions is widely distributed over devices because of gas diffusion [15–18].

On the other hand, negative ions appear to be locally produced in fairly large-sized plasmas existing in space environments and fusion-oriented confinement devices. Here, our attention is concentrated on plasma structure and dynamics associated with the local production of massive negative ions. Since no systematic investigation on this problem has been reported, to our knowledge, we have started to perform preliminary measurements [19–21] using a Q-machine plasma (quiescent-machine plasma, or contact-ionization plasma), where the fullerene C_{60} [22,23] is used for a massive negative ion source [24]. The Q-machine plasma, consisting of electrons and potassium positive ions K^+ (mass number $\simeq 39$), is produced by a thermal emission of electrons and contact ionization of potassium atoms on a high temperature (2300 K) tungsten plate under an electron-rich condition. The plasma density is about 1×10^9 cm^{-3} and the temperature of electrons T_e and positive ions T_+ are $T_e \simeq 0.2$ eV$\geqslant T_+$. When C_{60} molecules (mass number $\simeq 720$) with a relatively high electron affinity ($\simeq 2.7$ eV) [25,26] are introduced into this plasma, they become massive negative ions as a result of attachment of low-energy electrons ($C_{60} + e^- \rightarrow C_{60}^-$). The temperature of negative ions is $T_- \simeq 0.06$ eV. It is to be noticed that massive negative ions C_{60}^- are locally produced in the plasma column as a consequence of sublimation characteristic. C_{60} molecules (diameter $\sim 7\times 10^{-4}$ μm) are very small compared with the fine particle (diameter <10 μm) and the dust grain (diameter <100 μm), and their charge is restricted to $Z=1$ due to the size [27]. In this respect the massive negative ion plasma is strongly different from ordinary dusty plasmas.

In this paper we present results of a computer simulation, where the attention is focused on a self-excitation of fluctuations and a plasma state transition, etc., due to the local production of massive negative ions. A special emphasis is placed on a role of the solitary pulse in a particle ejection and a staying time distribution of charged particles, which denotes the feature of the state in the system. A part of this work on the dynamic evolution of plasma structures has been reported earlier in an abbreviated from Ref. [28].

II. SIMULATION MODEL

A computer simulation is performed by means of a one-dimensional electrostatic particle-in-cell (PIC) code which is based on an experimental configuration of Q machine, as shown schematically in Fig. 1. A grounded electrode as a plasma emitter (called a hot plate in the experiment) is situated at $z/\lambda_{Ds}=0$, and a floating electrode as a plasma termi-

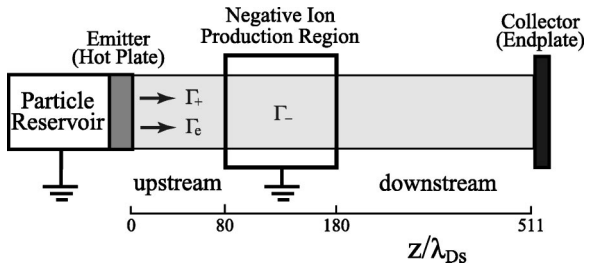

FIG. 1. Schematic diagram of simulation system, based on a Q-machine configuration. Negative ions are produced in the localized region $z_1 \leqslant z \leqslant z_2$. Γ_+, Γ_e, and Γ_- are particle fluxes of electrons, positive, and negative ions, respectively.

nator or a collector (called an endplate) is situated at $z/\lambda_{Ds}=511$. Here λ_{Ds} is the Debye length defined at a plasma source (a particle reservoir), and the subscript s implies the plasma source. All charged particles impinging on the electrodes are neutralized and removed from the system. Positive ions and electrons with half-Maxwellian velocity distributions are continuously supplied from the emitter into the plasma region. The mass and temperature ratios of positive ions to electrons are fixed to be $m_+/m_e=400$ (except for following Fig. 12) and $T_{+s}/T_{es}=1$ at the plasma source, respectively. The flux ratio of emitted electrons to positive ions, therefore, is $\Gamma_{es}/\Gamma_{+s}=(m_+/m_e)^{1/2}=20$. All the results are obtained with a time step $\omega_{ps}\Delta t=0.2$. Here ω_{ps} and Δt are the electron plasma frequency defined at the plasma source and the time step width, respectively. The number of particles per the Debye length at the plasma source is 1024.

In a localized region of the plasma ($80 \leqslant z/\lambda_{Ds} \leqslant 180$), some of electrons attach to C_{60} particles and are replaced by negative ions in the way that a total momentum is conserved ($m_- v_- = m_e v_e + m_{c_{60}} v_{c_{60}}$, $m_- = m_e + m_{c_{60}}$). Here ($m_-, m_e, m_{c_{60}}$) and ($v_-, v_e, v_{c_{60}}$) are masses and velocities of (negative ions, electrons, C_{60} particles), respectively. The mass ratio of negative ions to electrons is fixed to be $m_-/m_e=7360$ (except following Fig. 13) by taking into account $m_-/m_+=18.4$ in the experiment. The spatial distribution of C_{60} particles is assumed to be Gaussian with a central peak at $z/\lambda_{Ds}=130$, and the velocity distribution is assumed to be Maxwellian with the temperature ratio of C_{60} particles to electrons $T_{c_{60}}/T_{es}=0.29$. A production rate of negative ions α is defined $N_-/N_{se}=\alpha(N_e/N_{e0})$. N_- is the total number of negative ions produced, N_{se} is the total number of electrons supplied at $z/\lambda_{Ds}=0$, N_e and N_{es} are the total number of electrons in the production region ($80 \leqslant z/\lambda_{Ds} \leqslant 180$) with and without the negative ion production per unit time, respectively. N_{se} and N_{e0} are constant. N_- is proportional to N_e and changes temporally according to the situation of the plasma. An enlargement of α is qualitatively equivalent to raising the oven temperature for C_{60} sublimation and increasing the amount of C_{60} particles supplied in the experiment.

III. SIMULATION RESULTS AND DISCUSSION

A. State transition in plasma

When electrons and positive ions are emitted from the plasma emitter, they fill the system, providing a time-independent state ($\omega_{ps}t=0-14\times10^3$). Negative ions start to be produced at $\omega_{ps}t=14\times10^3$, the plasma becomes a regular state after time passes enough ($\omega_{ps}t>300\times10^3$). First of all, a general survey of the plasma state is described

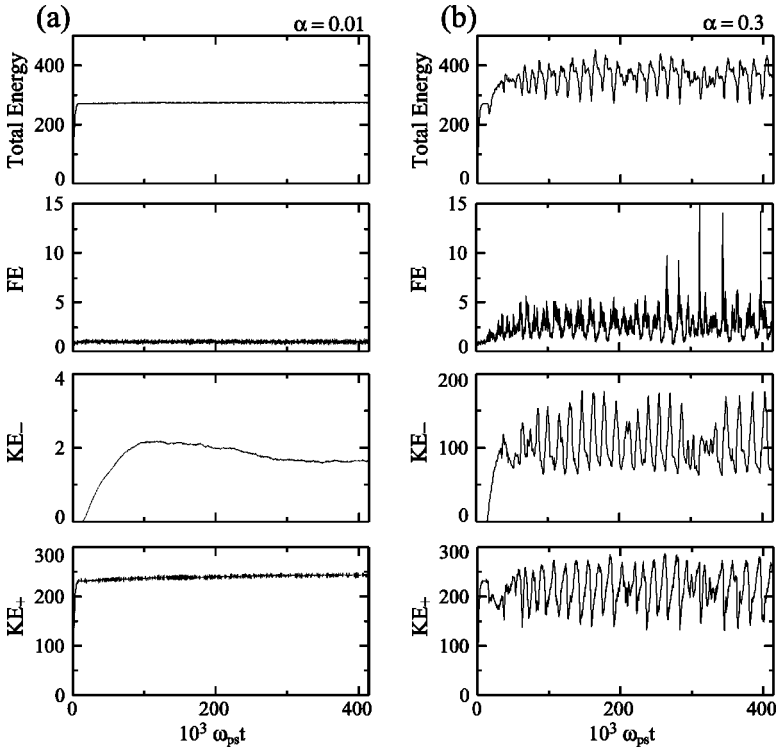

FIG. 2. Temporal evolutions of the total energy (top), the electric field energy FE (second from top), and the kinetic energies of all negative ions KE_- (third from top) and positive ions KE_+ (bottom) in the system for $\alpha=0.01$ (a) and 0.3 (b).

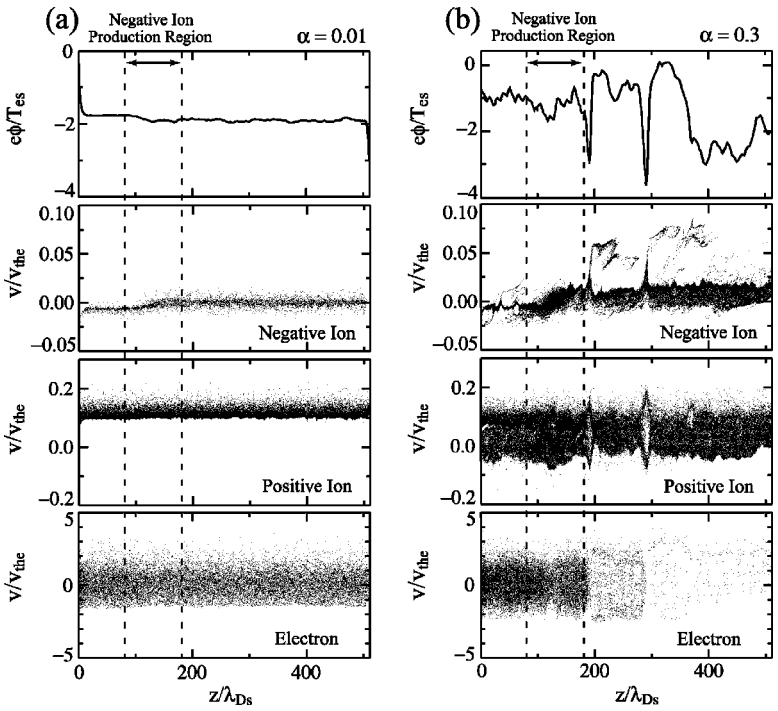

FIG. 3. Potential profile (top) and phase space distributions of negative ions (second from top), positive ions (third from top), and electrons (bottom) for $\alpha=0.01$ (a) and 0.3 (b).

by exemplifying two typical cases. Figure 2 shows temporal evolutions of the total energy (top), the electric field energy FE (second from top), and the kinetic energies of all the negative ions KE_- (third from top) and positive ions KE_+ (bottom) in the system for $\alpha=0.01$ (a) and 0.3 (b), respectively. The total energy in the system is a sum of FE, KE_-, KE_+, and KE_e (electron). A sheath is formed in front of the emitter to restrict the electron flux since the flux ratio of emitted electrons to positive ions is $\Gamma_{es}/\Gamma_{+s}=20>1$. Positive ions are accelerated in the sheath and form a beam in the plasma. The plasma is stationary in the regular state for a low rate of the negative ion production ($\alpha=0.01$) and the majority of the total energy is the drift energy of positive ions. For a high rate of the negative ion production ($\alpha=0.3$), however, a large fluctuation is found to appear in the physical quantities. The total energy starts to decrease intermittently at $\omega_{ps}t \sim 50\times 10^3$ after the initiation of the negative ion production. This is consistently attributed to a fact that the kinetic energy of negative ions KE_- is dumped outside the system, and the phenomena is described in detail as follows.

Figure 3 gives typical plasma profiles in the stationary state [$\alpha=0.01$, (a)] and the dynamic state [$\alpha=0.3$, (b)] at $\omega_{ps}t=386\times 10^3$, which are concerned with the potential ϕ (top) and the phase spaces of negative ions (second from top), positive ions (third from top), and electrons (bottom). Here v_{the} is the electron thermal velocity at the plasma source and the ϕ profiles are averaged over twice the electron plasma period ω_{ps}^{-1} defined at the plasma source. No remarkable modification of the potential profile [Fig. 3(a) top] is recognized for the low production rate ($\alpha=0.01$), but a small negative potential dip with a depth of $\Delta\phi$ ($e\Delta\phi/T_{es}\sim 0.1$) is almost stationarily formed at $z/\lambda_{Ds} \sim 130$. The produced negative ions diffuse to the upstream and downstream regions. Most of the negative ions are reflected in the sheath in front of the collector and return to the production region. Since some of them are reflected by the right side slope of the potential dip, negative ions with low kinetic energy remain for a long time in the downstream region. Therefore, the small potential dip contributes to the confinement of negative ions with low kinetic energy in the downstream region. The other negative ions are slightly accelerated by the left side slope of the potential dip and form a weak beam in the upstream region. A potential fluctuation with a small amplitude is excited by a two-stream instability between the weak beam of negative ions and the beam of positive ions, which flow in the opposite direction each other. For the high production rate ($\alpha=0.3$), pulses with negative potential are found in the downstream region. The pulse is called the solitary pulse as already found in the simulation and experimental results [19–21,28]. Negative ions are concentrated around them and positive ions with a low kinetic energy are trapped in the region of concave potential profile.

Based on the result of two typical plasma states described above, the plasma state dependence on the production rate α is now investigated in view of the fluctuation. Figure 4 shows (a) the temporal evolutions of the space potential ϕ and (b) the auto power spectrum of the potential fluctuation in the downstream ($z/\lambda_{Ds}=415$) for various values of α. When negative ions are not produced ($\alpha=0$), the spectrum has a frequency peak of $\omega/\omega_{ps}=0.43$ which corresponds to the electron plasma frequency. Since positive ions are accelerated in the sheath in front of the emitter, a ratio of the density in the plasma to that in the plasma source decreases down to 0.18, yielding an electron plasma frequency of $\omega_p/\omega_{ps}=0.43$. When α is gradually increased and negative ions are produced to some extent, two different states in the plasma, a stationary state and a dynamic state, are supposed to be achieved depending on α. The plasma is stationary for a low production rate ($\alpha\leqslant 0.05$), and no apparent fluctuation of low frequency ($\omega/\omega_{ps}<10^{-2}$) is observed, as seen in Fig.

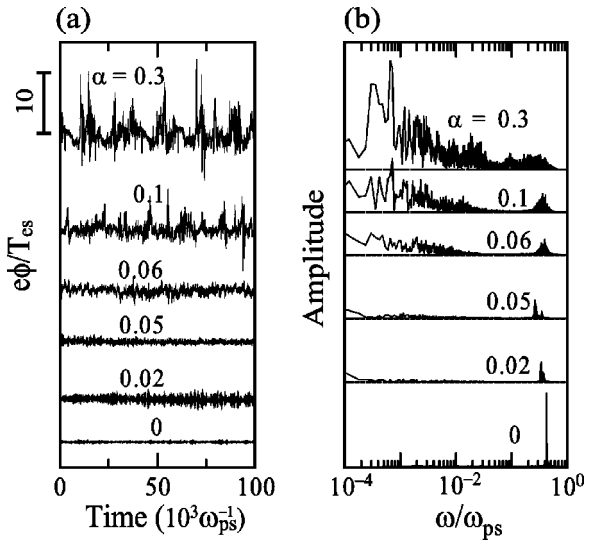

FIG. 4. Temporal evolutions and frequency spectra of space potential at $z/\lambda_{Ds}=415$ for various values of the production rate α of negative ions. Frequency $\omega/\omega_{ps}=0.43$ ($\alpha=0$) indicates the electron plasma frequency.

4(b). A transition from a stationary state to a dynamic state sharply occurs when α attains a critical value $\alpha_c(\sim 0.055)$. For a high production rate $\alpha>\alpha_c$, low frequency fluctuations and intermittent solitary pulses are excited in physical quantities, e.g., the space potential as shown in Fig. 4(a), the kinetic and field energies seen in Fig. 2(b), and all the particle numbers in the system.

Next, we refer to the excitation process of the fluctuations and the solitary pulses for a high production rate. Figure 5 presents spatiotemporal profiles of the space potential (a) and the densities of negative ions (b), electrons (c), and positive ions (d) during $\omega_{ps}t=(363\text{–}414)\times 10^3$ for $\alpha=0.3$. Here the dark color in the profiles of the potential and the densities denotes low potential places and high density places, respectively. It is found that the plasma structure is temporally modified in the entire system. A small-amplitude potential fluctuation is confirmed to be excited in the upstream ($z/\lambda_{Ds}\sim 50$) by the two-stream instability of positive and negative ions, as remarked above. When the generation condition of the two-stream instability is satisfied in the upstream, the background noise gains energy from positive ions and the small fluctuation is excited. The fluctuation approaches the upstream-side edge of the production region ($z/\lambda_{Ds}\sim 75$), and then the entire potential profile in the downstream is raised and the double layer is formed around the center of the production region. The negative dip of the fluctuation is rapidly enhanced, being transformed into a sharp pulse with negative potential. Electrons flowing toward the production region are reflected by this enhanced dip, and the positive-ion rich condition (charge separation) is attained just behind the dip as the dip depth becomes of the order of the electron temperature ($e\Delta\phi/T_{es}\sim 1$). Thus a large positive-potential difference behind the negative potential dip, a double layer, is formed [29]. The negative ion density is high at the position of the solitary pulse. Since a strong acceleration of negative ions by the potential gradient of the

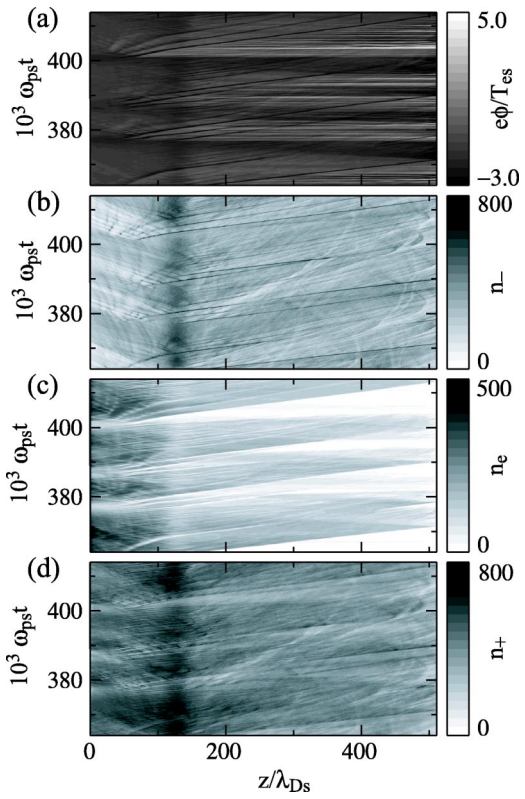

FIG. 5. Spatiotemporal profiles of space potential (a) and densities of negative ions (b), electrons (c), and positive ions (d) for $\alpha=0.3$.

double layer results in their bunching, the large-amplitude density pulse of negative ions is excited. While all the phenomena including excitation and propagation of the fluctuations and the solitary pulses are represented in the spatiotemporal profiles of Fig. 5, a more detailed excitation process of the solitary pulse is emphasized in Fig. 6. Short time evolutions of the potential profiles (a) and the phase space distributions of negative ions (b) at $\omega_{ps}t=400.8$ (top), 401.3 (second from top), 401.8 (third from top), and 402.5 (bottom) $\times 10^3$ are presented in Fig. 6. The solitary pulse has the amplitude $e\tilde{\phi}/T_{es}\sim 2$, which are intermittently excited at intervals with a period $14\times 10^3\omega_{ps}^{-1}$ (recall Fig. 2). The excitation period becomes short as α increases. The propagation speed toward the downstream is $4.7\times 10^{-2}v_{the}$ and is comparable to the pure negative-ion acoustic speed $c_{s-}\equiv\sqrt{3(T_+ + T_-)/m_-}\simeq 4.4\times 10^{-2}v_{the}$. This intermittent excitation of the solitary pulses is accompanied by the fluctuation excitation with the period of about $700\omega_{ps}^{-1}$. The propagation speed is $3.7\times 10^{-2}v_{the}$ and is smaller than the solitary-pulse speed.

The solitary pulse process of propagation toward the downstream and arrival at the collector is demonstrated in Fig. 7, which gives time evolutions of the potential profiles (a) and the phase space distributions of negative ions (b) at $\omega_{ps}t=411$ (top), 412 (second form top), 413 (third from top), and 414 (bottom) $\times 10^3$. Negative ions are usually reflected in the sheath formed in front of the collector. When the sheath changes markedly just before the solitary pulse

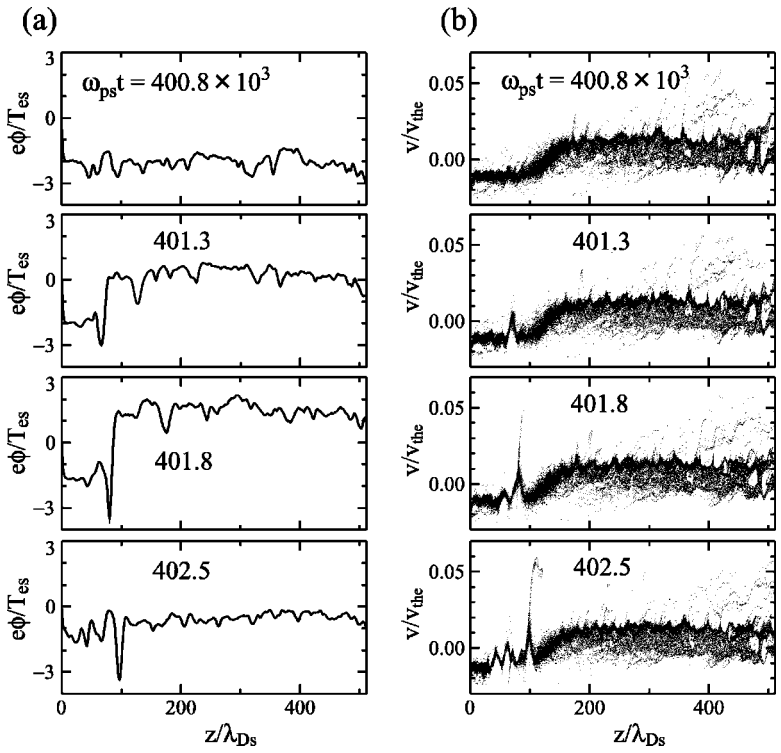

FIG. 6. Potential profiles (a) and phase space distributions of negative ions (b) at $\omega_{ps}t=400.8$ (top), 401.3 (second from top), 401.8 (third from top), and 402.5 (bottom) for $\alpha=0.3$.

arrives at the collector, however, a lot of negative ions can reach the collector ($\omega_{ps}t=413\times10^3$ in Fig. 7). Thus it can be said that the solitary pulse enhances the ejection of negative ions outside the system.

As described above, the feature of the plasma states before and after the state transition is chiefly taken notice of from the viewpoint of self-excitation of the solitary pulse and the fluctuation. Here we pay attention to the existence rate of negative ions, which is an unstable factor for the system, where the density profiles are different in each α according to the modification of the potential structure and the self-excited solitary pulses (fluctuations). Figure 8(a) shows time-averaged (during $50\times10^3\omega_{ps}^{-1}$) profiles of the density ratio ε of negative ions to positive ions ($\varepsilon\equiv n_-/n_+$, $n_+\simeq n_e+n_-:n_-$, n_+, and n_e are the densities of negative ions, positive ions, and electrons, respectively). The profiles in the

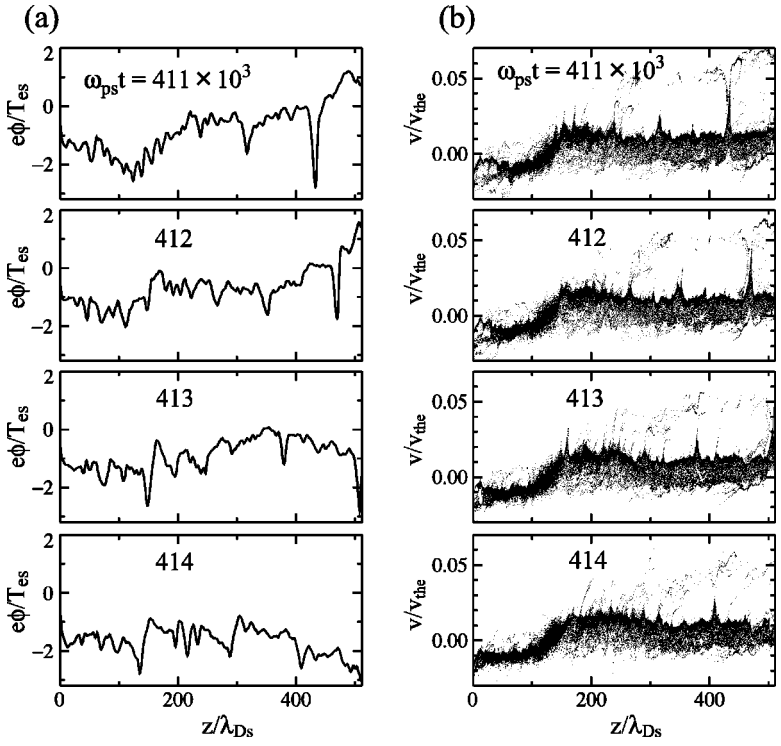

FIG. 7. Potential profiles (a) and phase space distributions of negative ions (b) at $\omega_{ps}t=411$ (top), 412 (second from top), 413 (third from top), and 414 (bottom) for $\alpha=0.3$.

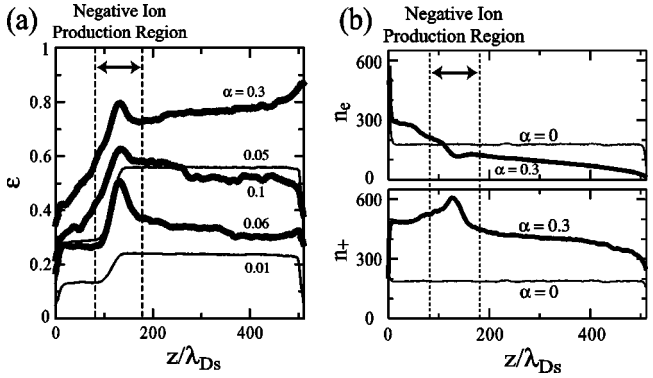

FIG. 8. Temporally averaged profiles of density ratio ε ($\equiv n_-/n_+$) of negative ions to positive ions for various α (a), and densities of electrons and positive ions for $\alpha=0$ and 0.3 (b).

cases of $\alpha \leqslant 0.05$ ($<\alpha_c$: stationary state) and $\alpha \geqslant 0.06$ ($>\alpha_c$: dynamic state) are denoted by fine and bold lines, respectively, where the production region of negative ions is indicated by an area between dashed lines ($80 \leqslant z/\lambda_{Ds} \leqslant 180$). Since some electrons flowing to the downstream are replaced by negative ions in the production region and negative ions spread through the upstream and the downstream regions, ε, i.e., the existence rate of negative ions, is comparatively high in the center of the production region. In the upstream region, the densities of electrons and positive ions are observed to increase because some electrons and positive ions flowing toward the downstream are reflected by the potential structures of the double layer and the solitary pulse, as seen in Fig. 8(b) for the typical values of $\alpha(=0,0.3)$. Thus ε in the upstream remains low compared with that in the downstream. The density ratio ε dependence on α in the upstream ($z/\lambda_{Ds}=65$) and the downstream ($z/\lambda_{Ds}=415$) regions is shown in Fig. 9. The majority of negative ions toward the downstream return to the production region in $\alpha < \alpha_c$ because they are reflected by the sheath in front of the collector, and ε in the downstream increases in proportion to α about twofold compared to that in the upstream. As already

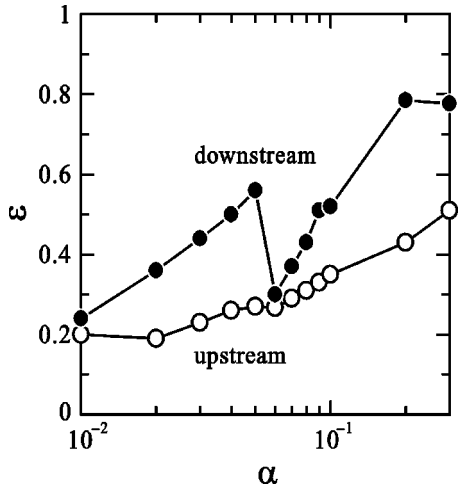

FIG. 9. Density ratio ε dependence on production rate α in upstream ($z/\lambda_{Ds}=65$) and downstream ($=415$).

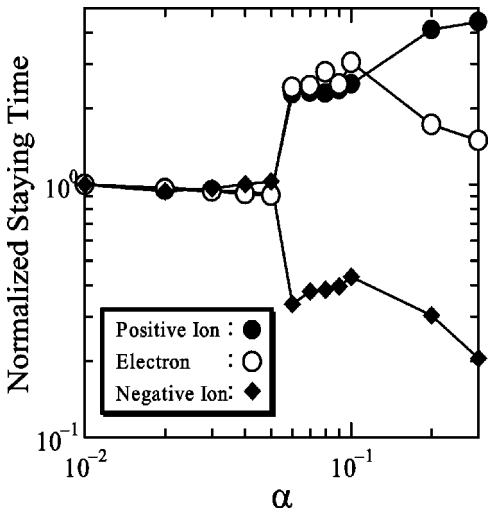

FIG. 10. Averaged staying times of charged particles as a function of the production rate α. The staying time is normalized by that for $\alpha=0.01$.

remarked upon the sheath drastically changes and a lot of negative ions are ejected to the collector when the solitary pulses are excited in $\alpha > \alpha_c$ and arrive at the collector. This is the reason why ε in the downstream greatly decreases for $\alpha \sim \alpha_c$. For $\alpha > \alpha_c$, ε in the downstream starts to increase in proportion to α, while ε in the upstream smoothly increases, because the number of negative ions produced increases. The reason for the difference of ε between in the downstream and the upstream is the same as that cited above in the case of $\alpha < \alpha_c$. It is noted here that the time-averaged numbers of supplied and ejected negative ions are balanced independently of α in the regular state. Even if α is different in Fig. 9, ε might be equal, for instance, ε's are almost equal for $\alpha=0.049$ and 0.09. Therefore, pursuing the argument based on only ε is not necessarily comprehensive and sufficient in order to indicate the feature of the plasma states clearly before and after the state transition. The features of the state of the system and the state transition cannot be specified only by physical variables concerning the numbers of particles, e.g., the densities of supplied and ejected particles. The state transition in an open system is a universal phenomenon, and details of the transition mechanism are quite different in each system. We have groped for a general index which is expected to indicate clearly the feature of the system.

B. Staying time distribution in plasma

For the purpose mentioned just above let us introduce the time τ_{st}, during which a charged particle stays in the system. τ_{st} is zero at the moment when a charged particle is supplied. Figure 10 shows the averaged staying time of all the particles as a function of α, which is normalized by that for $\alpha=0.01$. It is found that the averaged staying time sharply jumps and declines before and after $\alpha \sim \alpha_c$. Thus the staying time distributions averaged over $40\times10^3\omega_{ps}^{-1}$ are especially compared before and after the state transition in the cases of (a) negative ions $f_-(\tau_{st})$, (b) positive ions $f_+(\tau_{st})$, and (c)

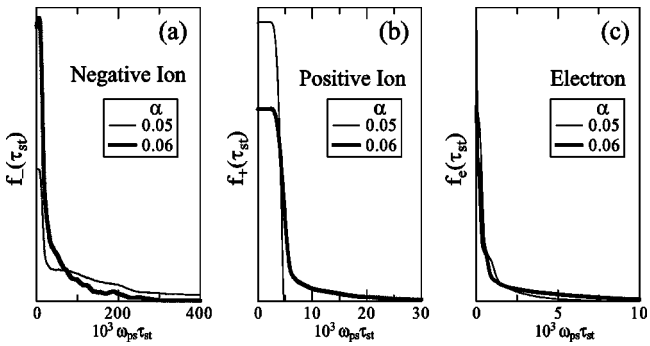

FIG. 11. Staying time distributions of (a) negative ions $f_-(\tau_{st})$, (b) positive ions $f_+(\tau_{st})$, and (c) electrons $f_e(\tau_{st})$ for $\alpha=0.05$ and 0.06, which are normalized by the total number of particles in the system.

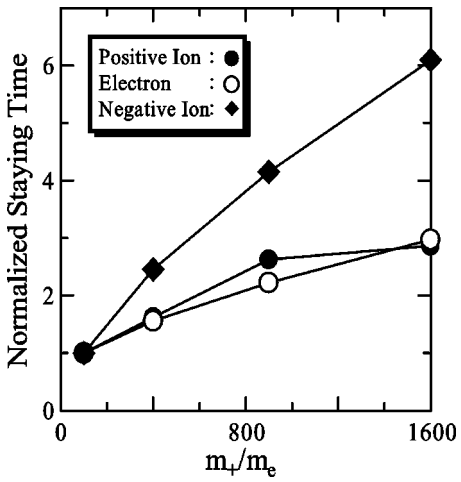

FIG. 12. Averaged staying times as a function of the mass ratio $m_+/m_e(m_-/m_+=18.4)$, which are normalized by those for $m_+/m_e=100$.

electrons $f_e(\tau_{st})$ for $\alpha=0.05$ (a stationary state, a fine line) and 0.06 (a dynamic state, a bold line), respectively, as shown in Fig. 11. The ordinate is normalized by the total number of the particles in the system. If a charged particle is replaced with a human in order to easily conjure up an image for a better understanding, the staying time corresponds to ''age'' for a human and the staying time distribution does to a ''human population pyramid.'' The number of negative ions with a long staying time ($\omega_{ps}\tau_{st}>100\times10^3$) for $\alpha=0.06$ is smaller than that for $\alpha=0.05$, namely, the averaged staying time in the case of $\alpha>\alpha_c$ is shorter than that in the case of $\alpha<\alpha_c$. This means that negative ions are ejected rapidly from the system when the system is in the dynamic state, and it can be said that the averaged longevity of negative ions becomes shortened, as also indicated in Fig. 10. On the other hand, the averaged staying times of positive ions and electrons increase after the state transition (also see Fig. 10), and that of positive ions especially increases as α increases in the case of $\alpha>\alpha_c$ [Fig. 11(b)]. Positive ions supplied from the emitter are accelerated by the sheath in front of the emitter, flow toward the downstream, and impinge on the collector in the stationary state. In the dynamic state, however, some of them are decelerated by the double layer formed transitionally, and positive ions with velocities smaller than the phase velocities of the solitary pulses and the fluctuations are trapped in their potential troughs. Accordingly, the averaged staying time of positive ions which are in disorder on the phase space ($\alpha=0.06$) comes to be longer than that in the case of one-pass flow ($\alpha=0.05$). As for electrons, the elongation of their averaged staying time is attributed to the reflection by potential dips of the double layer and the solitary pulse. All the phenomena generated in the system exert the influence on the history of the particle orbits and directly impact upon the staying time distribution (or the averaged staying time). Because the significant feature of the staying time distribution is successfully drawn by applying the averaged staying time, the following investigation is performed only in terms of the staying time.

By changing the masses of charged particles in negative ion plasmas we here clarify effects of the mass ratio on the features of the stability and the state transition. Figure 12 gives dependences of the staying time on the mass ratio of positive ions to electrons (m_+/m_e), where the mass ratio of negative ions to positive ions (m_-/m_+) is fixed at 18.4. In addition, dependences of the averaged staying time on m_-/m_+ are shown in Fig. 13, where m_+/m_e is fixed at 400. In Figs. 12 and 13 the production rate of negative ions is fixed at $\alpha=0.3$, and the averaged staying times are normalized by those for $m_+/m_e=100$ and $m_-/m_+=1$, respectively. In Fig. 12, it is confirmed from the analyes of the spatial and temporal plasma distributions and the frequency spectra of the potential fluctuations that the plasma for $\alpha=0.3$ remains the state after the transition and the system is unstable, promoting the ejection of negative ions for the case of $m_+/m_e=100$–1600. The staying times of positive ions and negative ions increase roughly in proportion to $0.1\sqrt{m_+/m_e}$ and $0.05\sqrt{m_-/m_e}$ ($0.2\sqrt{m_+/m_e}$), respectively. This is because the particle mobility becomes low as the mass ratio high if the kinetic energy is equal. It is interesting that the staying time of electrons increases though the mass of them does not change. When only the mass number of negative ions is increased, the staying times of negative ions and electrons hardly change, but on the other hand, the staying time of positive ions increases as shown in Fig. 13, where the plasma for $\alpha=0.3$ remains the state after the transition for the case of $m_-/m_+>1$, but before the transition for the case of $m_-/m_+=1$. When the mass number of negative ions increases, the negative ion mobility becomes low but the staying time of negative ions hardly changes regardless of m_-/m_+ because negative ions are promoted to ejection. Thus the staying time is not decided depending on only the particle mobility. It can be said that the staying time depends on the phenomena generated in the system, e.g., the self-excitation of fluctuation and the dynamic structural transformation. In view of these results, the staying time might be regarded as a general index which expresses the feature of the state independent of the details of physical mechanisms in open systems.

IV. CONCLUSIONS

A state transition between a stationary state and a dynamic state has been investigated in the case where massive

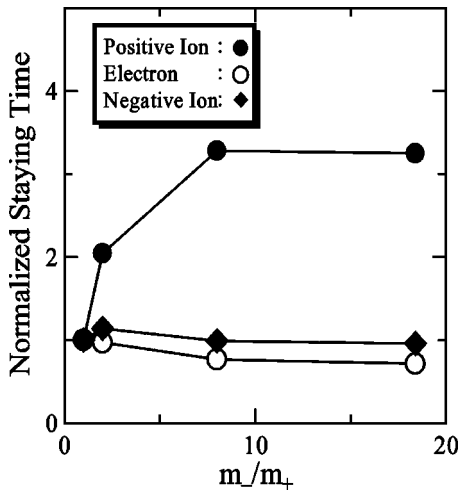

FIG. 13. Averaged staying times as a function of the mass ratio m_-/m_+ ($m_+/m_e=400$), which are normalized by those for $m_-/m_+=1$.

negative ions are locally produced in a collisionless plasma column. The state transition occurs depending on the production rate of negative ions, and solitary pulses and fluctuations are excited in the dynamic state. The solitary pulses modify potential structures including the sheath in front of a collector terminating the plasma column and a lot of negative ions toward the downstream can come to reach the collector easily. The solitary pulses play a crucial role in the rapid ejection of negative ions from the system. The staying time of a charged particle is introduced as an analog of age for a human. All the phenomena generated in the system directly reflect the staying time. Thus the averaged staying time of all the particles gives expression to the features of the state in an open system. Finally it is to be emphasized that the state transition and the instability in our open system essentially depend on the balance between the supply and ejection of massive negative ions rather than the existence of them distributed in the plasma.

ACKNOWLEDGMENTS

The authors would like to thank Professor Emeritus N. Sato for his encouragement. The computations were performed at the Advanced Computing System for Complexity Simulation at the National Institute for Fusion Science and at the computer center of Tohoku University in Japan. This work was supported by a Grant-Aid for Scientific Research from the Ministry of Education, Culture, Sports, Science and Technology, Japan.

[1] C.K. Goertz, Rev. Geophys. **27**, 271 (1989).
[2] T.W. Hartquist, O. Havnes, and G.E. Morfill, Fundam. Cosmic Phys. **15**, 107 (1992).
[3] F. Verheest, Space Sci. Rev. **77**, 267 (1996).
[4] H. Thomas, G.E. Morfill, V. Demmel, J. Goree, B. Feuerbacher, and D. Mohlmann, Phys. Rev. Lett. **73**, 652 (1994).
[5] J.H. Chu and I. Lin, Phys. Rev. Lett. **72**, 4009 (1994).
[6] Y. Hayashi and K. Tachibana, Jpn. J. Appl. Phys. **33**, 804 (1994).
[7] G.S. Selwyn, J.E. Heidenreich, and K.L. Haller, Appl. Phys. Lett. **57**, 1876 (1990).
[8] L. Boufendi, A. Bouchoule, P.K. Porteous, J.Ph. Blondeau, A. Plain, and C. Laure, J. Appl. Phys. **73**, 2160 (1993).
[9] B.M. Jelenkovic and A. Gallaghr, J. Appl. Phys. **82**, 1546 (1997).
[10] A. Gondhalekar, P.C. Stangeby, and J.D. Elder, Nucl. Fusion **34**, 247 (1994).
[11] B. Terreault, B.L. Stansfield, J.-L. Lachambre, R. Décoste, B.C. Gregory, E. Haddad, C. Janicki, C. Liu-Hinz, D. Michaud, A.H. Sarkissian, W.W. Zuzak, C. Boucher, A. Côté, F. Martin, H.H. Mai, G.G. Ross, M. St-Onge, and D. Whyte, Nucl. Fusion **34**, 777 (1994).
[12] J. Winter and G. Gebauer, J. Nucl. Mater. **266-269**, 228 (1999).
[13] B.N. Kolbasov, A.B. Kukushkin, V.A. Rantsev-Kartinov, and P.V. Romanov, Phys. Lett. A **269**, 363 (2000).
[14] R.L. Merlino, A. Barkan, C. Thompson, and N. D'Angelo, Plasma Phys. Controlled Fusion **39**, A421 (1997).
[15] A.Y. Wong, D.L. Mamas, and D. Arnush, Phys. Fluids **18**, 1489 (1975).
[16] B. Song, N. D'Angelo, and R.L. Merlino, Phys. Fluids B **3**, 284 (1991).
[17] N. Sato, in *A Variety of Plasmas*, edited by A. Sen and P. K. Kaw (Indian Academy of Sciences, Bangalore, 1989), p. 79.
[18] N. Sato, Plasma Sources Sci. Technol. **3**, 395 (1994).
[19] W. Oohara, S. Ishiguro, R. Hatakeyama, and N. Sato, in *Double Layers—Potential Formation and Related Nonlinear Phenomena in Plasmas*, edited by Sendai "Plasma Forum" (World Scientific, Singapore, 1997) p. 149.
[20] W. Oohara, R. Hatakeyama, S. Ishiguro, and N. Sato, *Proceedings of the 1998 Intl. Congress Plasma Physics, Praha, 1998* (European Physical Society, Paris, 1998), vol. 22C, p. 2419.
[21] W. Oohara, R. Hatakeyama, and S. Ishiguro, Plasma Phys. Controlled Fusion **44**, 1299 (2002).
[22] H.W. Kroto, J.R. Heath, S.C. O'Brien, R.F. Curl, and R.E. Smalley, Nature (London) **318**, 162 (1985).
[23] W. Krätschmer, L.D. Lamb, K. Fostiropoulos, and D.R. Huffman, Nature (London) **347**, 354 (1990).
[24] N. Sato, T. Mieno, T. Hirata, Y. Yagi, R. Hatakeyama, and S. Iizuka, Phys. Plasmas **1**, 3480 (1994).
[25] T. Jaffke, E. Illenberger, M. Lezius, S. Matejcik, D. Smith, and T.D. Märk, Chem. Phys. Lett. **226**, 213 (1994).
[26] J. Huang, H.S. Carman, Jr., and R.N. Compton, J. Phys. Chem. **99**, 1719 (1995).
[27] T. Fukuzawa, M. Shiratani, and Y. Watanabe, Appl. Phys. Lett. **64**, 3098 (1994).
[28] W. Oohara, S. Ishiguro, R. Hatakeyama, and N. Sato, J. Phys. Soc. Jpn. **71**, 373 (2002).
[29] A. Hasegawa and T. Sato, Phys. Fluids **25**, 632 (1982).